full page ad

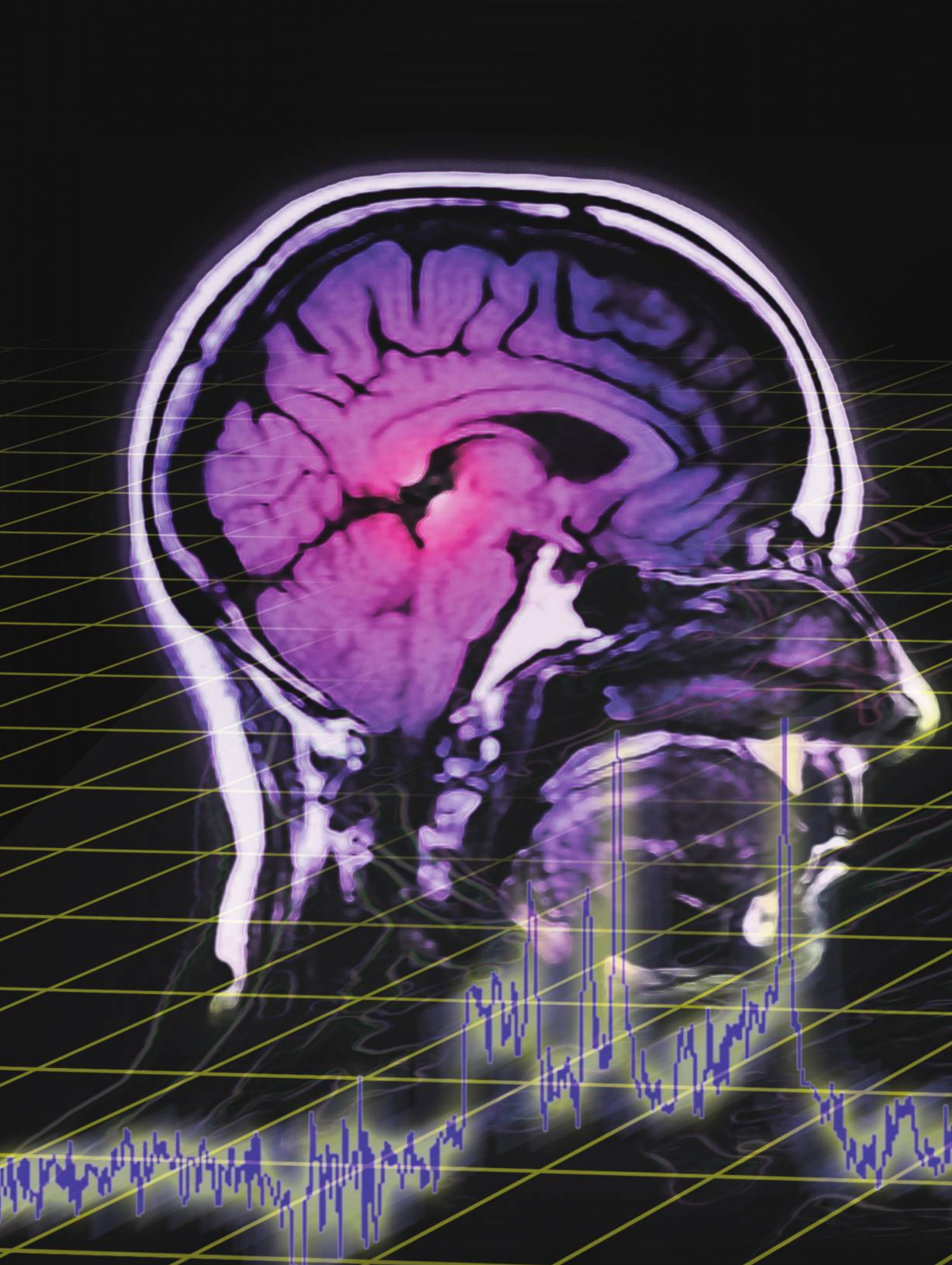

# Better Brain Imaging with Chemometrics

## Mathematical methods could improve noninvasive techniques that distinguish brain tumors from healthy tissue.

One of the many tangential benefits of the computer revolution has been the development of chemometrics, which has been adopted for many applications in analytical chemistry. Chemometrics uses statistical and mathematical methods to unravel chemical problems. As described in various textbooks, chemometrics plays a decisive role in process analytical chemistry, both in monitoring and control applications, and is increasingly used in areas such as analyzing images and optimizing molecular structures on the basis of their properties and activities (*1–4*).

Nuclear magnetic resonance (NMR) of molecules in living tissue is a new challenge for chemometrics. NMR can be performed as either spectroscopy

**Han Witjes, Arjan W. Simonetti, Lutgarde Buydens**
*University of Nijmegen (The Netherlands)*

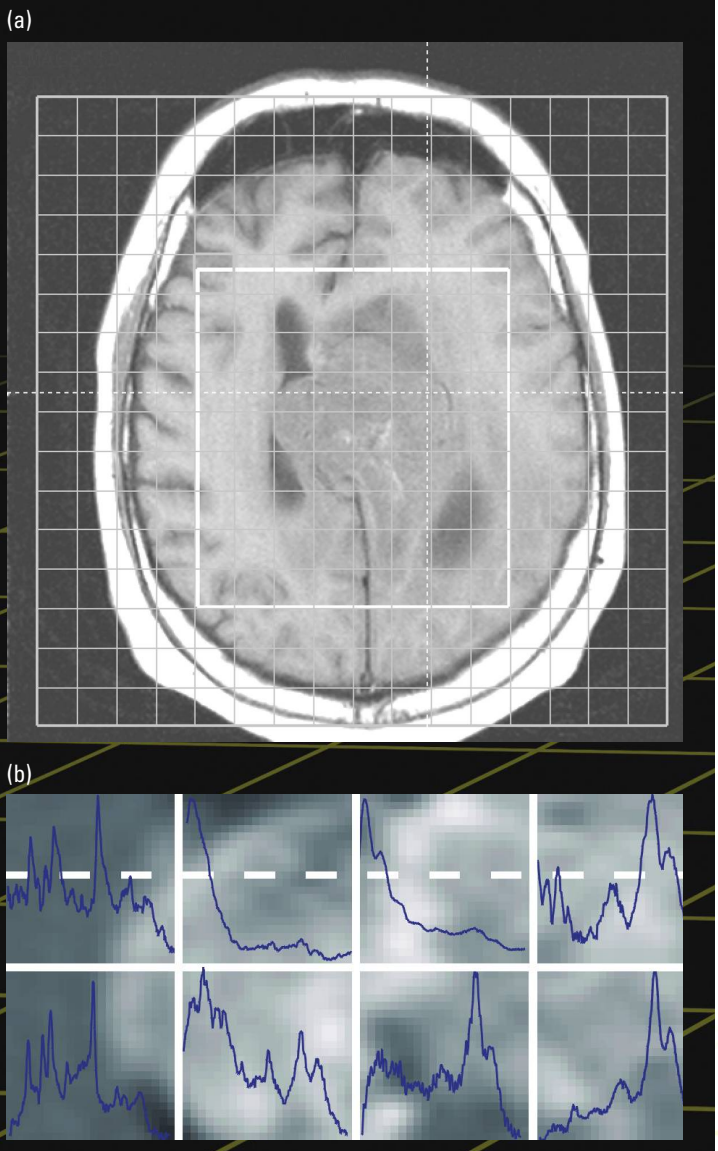


**FIGURE 1.** MR data acquired from a cross-sectional image slice through the brain tumor.

(a) The MR image shows the proton NMR signal of water on a high spatial resolution. The grid indicates the lower spatial resolution of the spectroscopic image. (b) Part of the spectroscopic image showing the MR spectra from adjacent spectroscopic voxels in the tumor region. Each spectrum shows the proton NMR signal of various metabolites like NAA, Cho, and Cr. The differences between the spectra of adjacent spectroscopic voxels in the MR spectra indicate the large tissue heterogeneity of the brain tumor.

(MRS) or imaging (MRI). (The term "nuclear" is omitted in a clinical environment because it is often incorrectly associated with nuclear radiation.) MRI is an established medical technique for examining different internal organs like the brain, prostate, and heart and is an accepted clinical tool for imaging blood vessels and musculoskeletal tissue.

In particular, MRI is the most useful imaging modality for examining brain tumors. Acquiring MR images of representative cross-sectional slices of the head to detect and localize a brain tumor is a daily occurrence. One or more small tissue samples called biopsies are then removed from the localized tumor to determine identity and grade. Depending on the diagnosis, a patient next receives chemotherapy, radiation treatment, or undergoes surgery. However, a biopsy is far from optimal for the diagnosis of brain tumors because it is invasive, subject to sampling errors, and provides no information about the tissue heterogeneity of the tumor. Therefore, MRI, MRS, and a combination of these techniques called magnetic resonance spectroscopic imaging (MRSI) are being explored in clinical trials in the hope of providing noninvasive brain tumor diagnoses.

Here lies the major challenge for chemometrics: No breakthroughs are expected in clinical MR examinations of brain tumor patients because analysis and interpretation of the acquired MR data are still the major bottleneck. But the combination of MRI, MRSI, and chemometrics may advance the fast, noninvasive diagnosis of brain tumors.

In this feature, we will explain some basic elements of MRI and MRSI in human brain studies and focus on the possibilities and added value that chemometrics can offer the techniques.

## MRI basics

Figure 1a is an MR image that shows the spatial distribution of the proton NMR signal of water in a cross-sectional tissue slice of a human brain tumor. The voxel (volume element) of each pixel in an image is ~0.01 $cm^3$.

Manipulating the MR image contrast by varying acquisition parameters has proven to be MRI's greatest strength. The spin-echo imaging technique is used routinely in the clinical environment to collect data. Just like any other MR sequence, spin-echo imaging uses radio frequency (rf) pulses and magnetic field gradients, which are applied to a subject placed inside a homogeneous static magnetic field. The pulse sequence generates the proton NMR signal, while the gradient sequence spatially encodes the proton NMR signal.

The proton density (ρ) and the spin–lattice ($T_1$) and spin–spin ($T_2$) relaxation times are parameters that determine the NMR intensities of the different tissue types. The echo time (*TE*) and the repetition time (*TR*) are acquisition parameters that determine the ρ-, $T_1$-, and $T_2$-sensitivity of the acquired spin-echo images. According to Equation 1, the signal intensity (*S*) in each voxel can be described to a first-order approximation (assuming that *TR* >> *TE*) as

$$S = \rho \cdot [1 - \exp(-TR/T_1)] \cdot \exp(-TE/T_2) \qquad (1)$$

*S* is heavily ρ-weighted if *TR* is long with respect to $T_1$ and *TE* is short with respect to $T_2$, $T_2$-weighted if *TR* is long and *TE* is long, and $T_1$-weighted if *TR* is short and *TE* is long. Thus, on

the basis of a tissue's ρ, $T_1$, or $T_2$ values, different intensities are recorded in the ρ-, $T_1$-, or $T_2$-weighted images.

In the hospital, the ρ-, $T_1$-, and $T_2$-weighted images are commonly acquired with the spin-echo technique for different combinations of *TE* and *TR*. These images are usually combined for normal brain tissue segmentation, which is the discrimination between white matter, gray matter, and cerebrospinal fluid. However, additional feature images are required for the segmentation of the different tissue types in the image within a tumor bed. A contrast agent is usually introduced to the patient before collecting a $T_1$-weighted spin-echo image. The contrast agent shortens the $T_1$ of brain tissue, which has a disrupted vascular structure as a result of tumor proliferation.

## Understanding MRSI of brain tumors

Figure 1b is an MR spectroscopic image that shows the spatial distribution of the proton NMR signal of various metabolites in a cross-sectional tissue slice of a human tumor. The voxel size in an MR spectroscopic image has to be ~1 $cm^3$ to acquire proton NMR signals of metabolites with an adequate S/N. In addition, only metabolites with concentrations >0.1 mM are visible in the MR spectrum. A spin-echo-based pulse sequence in combination with additional pulses is often used in MRSI to suppress the large proton signals of water and possible fat that would spoil the spectrum (*5*).

Proton signals for metabolite markers *N*-acetyl-aspartate (NAA), phosphocreatine and creatine combined (Cr), choline-containing compounds (Cho), and lactate (Lac) can be observed in spatially resolved MR spectra. The metabolite levels in tumor and normal brain tissue are quite different. For example, the concentration of NAA, a neuronal marker, is low in tumor tissue because tumors characteristically lose neuronal cells. Cho is elevated in tumor tissue because membrane synthesis and degradation increases. The Cr signal is reduced or even absent in tumor spectra because of the reduced energy metabolism in tumor tissue. Lac is usually observed in tumor spectra because it indirectly marks abnormal glycolysis. Thus, these metabolite levels, as reflected by the MR signal intensities, provide potential markers for tumor identity and grade.

However, the observed signal intensities in the MR spectra may not directly reflect the relative concentrations of the metabolites present in the spectroscopic voxels. Different combinations of *TE* and *TR* yield different spectral profiles in the voxels because the various metabolites have different $T_1$ and $T_2$ values. Only MR spectra of voxels acquired at identical combinations of *TE* and *TR* can be compared for characterization. Usually, short echo- or long echo-time spectra are acquired.

The acquisition of short echo-time spectra reduces the signal loss due to $T_2$. This means that spectra with higher S/N are obtained, and additional resonance peaks of metabolites with short $T_2$ values such as *myo*-inositol, glutamate, and glutamine are detected, which may be disease markers. On the other hand, a broad background signal appears in the spectra from macromolecules with short $T_2$ values. Although short echo-time spectra provide more biochemical information, they are more difficult to analyze and interpret because of the broad peaks from short $T_2$ macromolecules.

## Diagnosing brain tumors

MRI and MRSI will irrevocably improve patient diagnosis and treatment if viable tumor tissue can be distinguished from abnormal, nonmalignant tissue types, such as necrosis, edema, and possibly radiation necrosis and scar tissue, within the tumor bed. Moreover, the delineation of a viable tumor will facilitate noninvasive diagnosis or at least guide the collection of biopsies, aid the study of the effects of chemotherapy or radiation treatment over time, and help monitor patients after surgery.

The standard ρ-, $T_1$-, and $T_2$-weighted MR images hardly allow proper tissue discrimination within the tumor region. Contrast agents enhance lesion-imaging in areas where the blood–brain barrier is damaged. This barrier may be affected to various degrees, and the extent of the tumor tissue may be under- or overestimated. If there is a significant leak in the blood–brain barrier, then blood will flow through the surrounding healthy tissue and lead to an overestimation of tumor area. Tumors are underestimated if the barrier is damaged only slightly. The blood will stay in the vessels, and the tumor can hardly be seen in the image.

**MRI is the most useful imaging modality for examining brain tumors.**

Combined MRI/MRSI studies have revealed that images of a contrast-enhanced lesion are much smaller than the region of actual abnormal metabolism (*6*). MRSI studies found that metabolite levels vary widely for individual tumors. Large standard deviations in metabolite levels of one tumor type and substantial overlap of metabolite levels between different tumor grades have been measured (*6*). Other studies showed clear differences between necrosis and other abnormal tissue, although these studies are limited by low spatial resolution (*6*). Because MRSI and MRI are complementary techniques, chemometrics should facilitate the fusion of morphologic (MRI) and metabolic (MRSI) data to improve the delineation of brain tumors.

The data analysis methodology must quickly process the large stream of MRI and MRSI data and deal with difficulties. Due to time constraints, spectroscopic images with low S/N are typically acquired. Moreover, a patient can move during MR acquisition, and the resulting artifacts may complicate the data analysis. In vivo examinations also hamper any form of "sample

preparation" that would facilitate data analysis. Therefore, MR examinations of brain tumor patients are, to a large extent, dependent on proper data processing.

A chemometric methodology will only be accepted in the clinical environment if it produces reliable results with minimal subjective user interaction. Laboratory assistants are usually unfamiliar with sophisticated data analysis techniques. The simplicity and transparency of the data analysis methodology is crucial for its implementation in a hospital.

## Processing MR images

***Image registration.*** Image registration, also called image matching, compensates for patient movement during the MR examination or combines images from serial MR examinations of a single patient. Serial MR examinations are performed to study tumor growth or shrinkage after radiation treatment. A suitable registration algorithm should be able to quickly detect the same tissue slice as the one previously measured.

Precautions are taken to restrict the movement of the head during an MR examination of a brain tumor patient. Therefore, patient movement results in only small shifts, which can be corrected with a simple cross-correlation method between different images (*7*). However, a disadvantage of cross-correlation methods is their sensitivity to intensity differences in different contrast images. Feature-based registration methods can help the radiologist find the target position of the tissue slice in serial brain tumor MR examinations. These methods align images by translational, rotational, and uniform scaling transformations.

Previous registration points that are insensitive to changes in tissue and acquisition conditions, for example, edges and corners in normal brain tissue regions, are sought for matching. Then a suitable algorithm like the Procrustes algorithm can be used to find the least-squares solution by minimizing the distance among all paired points in the two images (*8*). The execution time of the algorithm linearly decreases with the number of registration points used. Multiscale approaches using wavelets have been proposed to increase the computation speed of registration algorithms. With wavelet analysis, image representations on different spatial resolutions allow the sampling of fewer registration points sufficient for adequate registration (*9*).

***Removal of nonbrain tissue.*** Image segmentation of brain tissue is simplified if nonbrain material such as bone, skull, face muscles, and air is removed from the images. The removal of these materials can simply be achieved by drawing a region of interest in the image containing only brain tissue. A simple algorithm for the automatic removal of skull tissue and air is presented in Ref. 10. The method is based on the construction of a radius image with the ρ-weighted image, because ρ-weighting clearly defines the transition between brain tissue and skull. The ρ-weighted image can subsequently be used as a mask image to remove skull tissue and air outside the brain from other registered contrast images. Another accepted method that requires minimal user intervention to remove the skull from the image is based on a multiresolution algorithm (*11, 12*).

***Image filtering.*** Image filtering is applied in brain MR imaging of tissue slices thinner than 1 cm to ensure low S/N ratios. A popular MR image filter is the nonlinear anisotropic diffusion filter, which improves the S/N without blurring the fine structural details in the image (*13, 14*).

***Field inhomogeneity correction.*** Magnetic field inhomogeneities decrease the digitized signal amplitude (pixel intensity) of a voxel. For example, in a typical MR scan, the inhomogeneous static magnetic field ($B_0$) of the scanner broadens the water resonance peak because the resonance frequency is proportional to the strength of the applied magnetic field, resulting in a decrease in pixel intensity. Usually, the spatial inhomogeneity of this field is negligible.

However, the spatial inhomogeneity of the rf magnetic field ($B_1$) produced by the coil surrounding the head may be significant. The coil excites proton spins and receives the proton signal of a selected tissue slice. Regional field strength differences inside the coil are caused by inhomogeneities in rf coil sensitivity and rf transmission. The nonuniform excitation and reception profiles of the coil yield nonuniform intensity variations across the image, which depend on the coil design, slice orientation, pulse sequence, and even the patient. The nonuniformity appears as a low spatial frequency component in the image and is commonly removed by two-

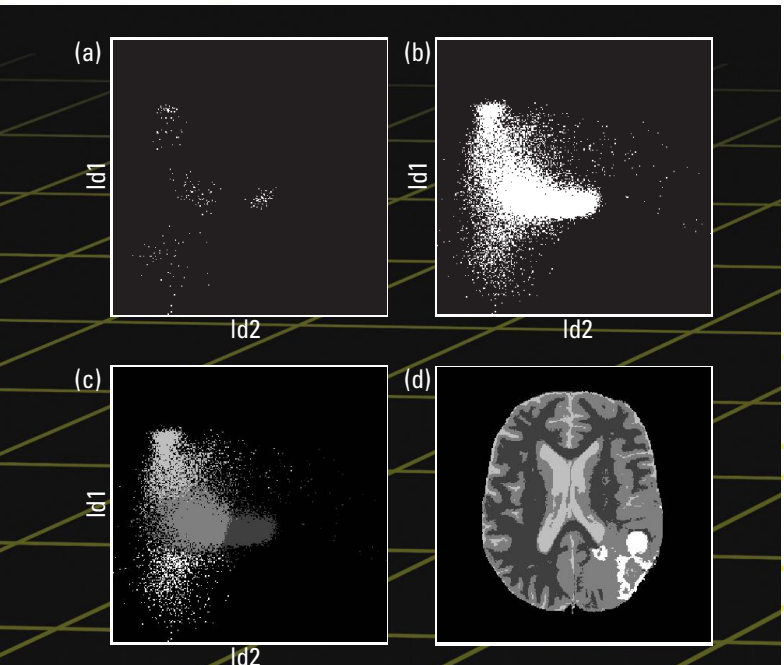


**FIGURE 2.** LDA applied to the segmentation of a multivariate image.

(a) Discriminant scores of the training pixels for white matter, gray matter, cerebrospinal fluid, and tumor in the ld1–ld2 score plot. (b) Discriminant scores of all pixels in the same ld1–ld2 score plot. (c) Classification of all pixels based on the Euclidean distance: The shortest distance to a class center determines the class membership of the pixel. (d) Classification of all pixels shown in the corresponding image domain. The tissue classes are color-coded: White is tumor, light gray is cerebrospinal fluid, gray is gray matter, and dark gray is white matter.

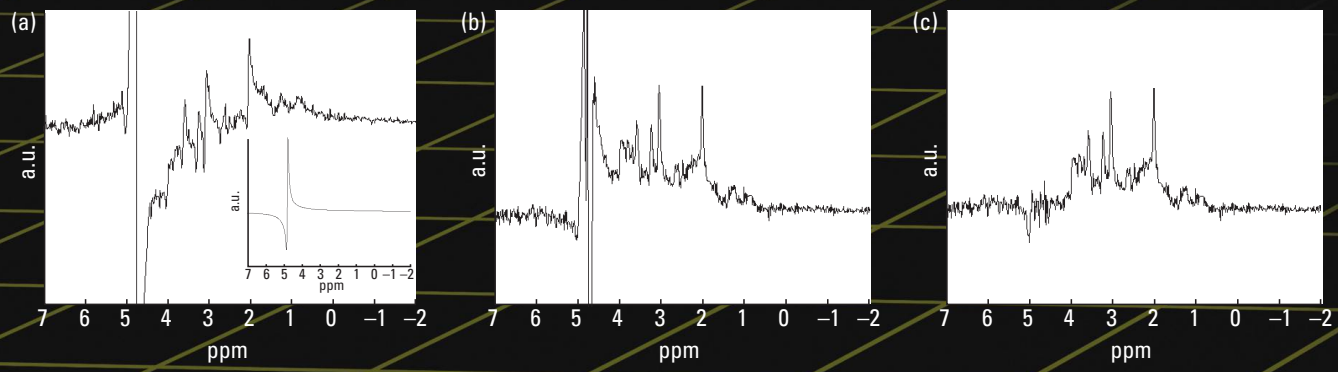


**FIGURE 3.** (a) Water-suppressed in vivo MR spectrum acquired from a voxel in the human brain. (inset) Water-unsuppressed spectrum from the same voxel. Water suppression is accomplished by using additional rf pulses to saturate the water resonance. (b) After eddy current correction of (a), demonstrating that the metabolite peaks are phased with the phase of the water peak. (c) After filtering the residual water peak at 4.7 ppm of (b).

dimensional (2-D) low-pass filtering, which is distinct from S/N ratio improvement.

An experimental method to correct for image nonuniformity is to image a test sample with a uniform NMR intensity across the field of view with the coil surrounding the patient's head. A phantom filled with water is usually imaged for this purpose (*15*). The correction coefficients for producing uniform intensity images of the sample are stored in the computer and subsequently applied to patient brain MR images. An important disadvantage of this method is that the rf penetration through the sample is not the same as of the patient.

***Multivariate image segmentation.*** A multivariate image consists of a series of MR images of the same tissue slice such as ρ-, $T_1$-, and $T_2$-weighted MR images. In this case, segmentation means dividing a multivariate image into regions of different tissue types. Multivariate image segmentation starts after removal of nonbrain tissue and, if necessary, after image registration, field inhomogeneity correction, and image noise removal.

The simplest use of multivariate image segmentation is to combine two registered MR images. For each pixel, the intensity in one image is plotted against the intensity in the other image to define a 2-D variable, or feature space. Image segmentation is achieved by defining regions in the 2-D feature space corresponding to the different tissue types. In case of three registered images, a 3-D feature space can be defined in which the different tissue types are located at different positions. However, this approach becomes more difficult if more than three registered images need to be combined. The lack of visual inspection complicates the isolation of different clusters corresponding to different tissue types in the multidimensional feature space. Pattern recognition techniques, an important area of chemometrics, have been used to deal with this problem.

Principal component analysis (PCA) is the most popular technique in the field of chemometrics and has been used in the visualization of multivariate image data (*16*). PCA transforms a set of registered MR images into a new set of abstract images, called the PCA score images, in such a way that the image contrast information is condensed into the first few PCA score images (*17*). By defining a 2-D feature space with the first two PCA score images, an expert can delineate the different tissue regions in this 2-D plot based on 80–90% of the image contrast variance present in the set of MR images.

However, due to possible field inhomogeneities and the partial volume effect, also referred to as the mixing effect of multiple tissue types within one voxel, no distinct groups of pixels appear in the 2-D PCA score plot. In fact, no dedicated technique to date is able to reduce the dimension of multivariate MR images in such a way that distinct tissue clusters can be visualized. User interaction is required to improve the segmentation of multivariate brain MR images. Supervised pattern recognition methods such as discriminant analysis, neural networks, and fuzzy clustering methods have been applied to the segmentation of multivariate MR images. However, these methods may also produce misleading segmentation results because of the subjectivity of the user input. Therefore, PCA is still a valuable tool for visualizing and exploring multivariate images because it requires no user input.

Linear discriminant analysis (LDA) is the best-known technique for supervised pattern recognition. LDA can use a sub-

**Tumors are underestimated if the barrier is damaged only slightly.**

set of pixels of known tissue type, called a training set, to calculate a classification model. It maximizes the ratio of the between-class and within-class variance of the tissue classes present in the training set using linear combinations of the original MR images. The calculated discriminant axes (lds), linear combinations of the MR images, discriminate between the tissue classes defined in the training set. The first discriminant axis (ld1) has the largest discriminative power, the next discriminant axes show less discriminative power with increasing ld number. The use of LDA in multivariate image segmentation is illustrated in Figure 2.

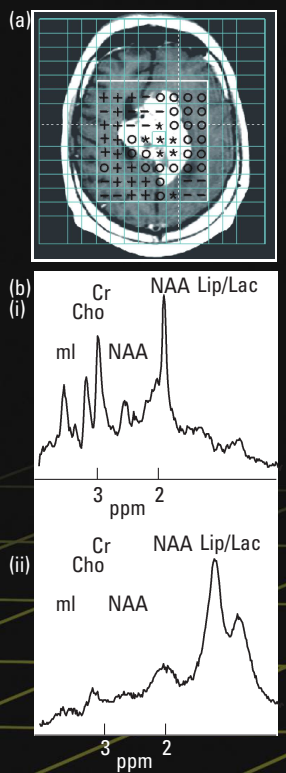


**FIGURE 4.** (a) (background) Gadolinium-enhanced $T_1$-weighted MR image of a brain tumor; (foreground) grid of spectroscopic voxels. The symbols indicate the group membership of each spectrum, as determined with hierarchical cluster analysis. (b) Two of the MR spectra of the spectroscopic image: (i) Likely originates from a healthy region; (ii) from a malignant tumor region. The six quantifiable resonances are indicated: *myo*-inositol (ml) at 3.6 ppm, choline (Cho) at 3.2 ppm, creatine (Cr) at 3.0 ppm, *N*-acetyl aspartate (NAA) at 2.6 and 2.0 ppm, and lipids/lactate (Lip/Lac) at 1.3 ppm.

As in any segmentation technique requiring user input, the training pixels need to be selected by a human interpreter. Different operators will select different training sets (creating inter-observer variations) at different times (creating intra-observer variations), resulting in different segmented images or tissue maps. A radiologist has to assess the quality of these calculated tissue maps because there is no definitive method that can verify the segmentation results, which is a fundamental problem in medical image processing. Therefore, segmentation performance is usually determined by the consistency or sensitivity to operator input of the applied method, not by the accuracy of image segmentation. Several studies have shown that the segmentation of brain tumors strongly depends on method and training data (*18–20*). The major challenge is to develop novel multivariate segmentation techniques that minimize operator input but are robust enough to withstand small variations in input.

## Processing MR spectroscopic images

***Eddy current correction.*** Switching magnetic field gradients induces small currents in the magnet system called eddy currents. These time-dependent currents disturb the field homogeneity and cause time-dependent frequency shifts of the resonances in the selected voxel. This results in a distortion of the spectrum after Fourier transformation of the time signal. Unlike MRI, MRSI suffers from eddy currents because of the low signal intensity of the metabolite resonances. Therefore, to remove eddy current distortions, both water-suppressed and water-unsuppressed MRS images of a selected tissue slice are acquired in a single MRSI examination, as shown in Figure 3a.

For each voxel, eddy current distortions are corrected in the time domain by dividing the water-suppressed signal by the phase factor of the water signal for each data point. The influence of metabolite protons in the water-unsuppressed MRS image is negligible (*21*). Figure 3b demonstrates a spectrum corrected for eddy currents that is aligned in phase and in spectral position to the water resonance peak within the voxel.

***Residual water filtering.*** The MR spectrum corrected for eddy currents in Figure 3b still contains a residual water peak. This intense peak is usually filtered with a Hankel Lanczos singular value decomposition (*22*). The first few singular values account for the intense water resonance and are subtracted from the spectrum. The algorithm is applied in the time domain to remove the long tails of the water peak that overlap some of the metabolite peaks in the spectrum. The result of residual water filtering of the MR spectrum in Figure 3b is shown in Figure 3c.

***Phase and frequency shift correction.*** Small phase differences between metabolite peaks in the MR spectrum remain after eddy current correction. These remaining phase shifts are frequency-dependent (first-order). Phase correction provides complete absorption-mode spectra, which make interpretation and analysis of the spectra easier. Interactive phase-correction facilities are standard on MR instruments; however, fast and automatic phasing is desirable for processing the large number of spectra and obtaining unbiased results.

Frequency shifts, or peak shifts between spectra of different voxels, may also distort further spectra analysis. Although frequency shifts induced by the spatial inhomogeneity of the rf field are removed by eddy current correction, patient movement between the acquisition of water-unsuppressed and water-suppressed MRSI data may induce them. Patient movement changes the coil loading, deteriorating the spatial homogeneity of the rf field inside the coil. A novel method has recently been developed for quickly removing phase and frequency shifts across a large series of single-resonance peaks (*23*). The method works well on noisy and distorted MR spectra acquired under in vivo conditions.

***Pattern recognition.*** After preprocessing, MR spectra can be classified according to their tissue identity. It is impossible to categorize the processed MR spectra with respect to tissue identity by visual inspection of the data, which makes pattern recognition methods indispensable. These methods cluster the spectra based on their mutual characteristics.

Selecting spectral features that provide the best discrimination are important considerations when designing a pattern recognition model. For the pattern recognition of brain MR spectra, estimated levels of metabolites are used rather than the complete

spectrum. The relative levels of NAA, Cho, and Cr are derived from long echo-time spectra by curve-fitting routines. Estimation considerably reduces the dimension of the input data, and spectral noise is omitted in the pattern recognition.

Metabolite levels from short echo-time spectra are much harder to estimate. These spectra are contaminated with broad peaks of nonrelevant macromolecules that distort the classification performance. Short echo-time spectra are usually fit in the time domain and are advantageous because complicated model functions, similar to the measure peak shapes, can be used. For example, the useful Voigt function can only be approximated in the frequency domain or must be calculated by numerical integration (*24*). Nonlinear iterative optimization methods such as the Levenberg–Marquardt algorithm (*25*) are preferred in spectral fitting. These methods allow any mathematical form of the model function to be used for fitting the spectra, including the Voigt function.

Moreover, prior knowledge of, for example, spectral position and relative amplitudes can be incorporated into the model function and improve the quantification of resonance peaks (*26*). Recently, novel quantitation methods have been developed that operate on a complete series of MR spectra instead of on each separately (*23, 27, 28*). These have been proposed for the fast and accurate quantitation of resonances in series of relatively simple in vivo MR spectra.

Figure 4a demonstrates the pattern recognition of a spectroscopic image of a patient with a brain tumor. Figure 4b gives two of the MR spectra acquired from the patient's brain. The six resonance peaks labeled in the spectra were quantified and subsequently normalized to the unsuppressed water signal within the voxel. These normalized peaks define the input vector for the pattern recognizer for each spectrum.

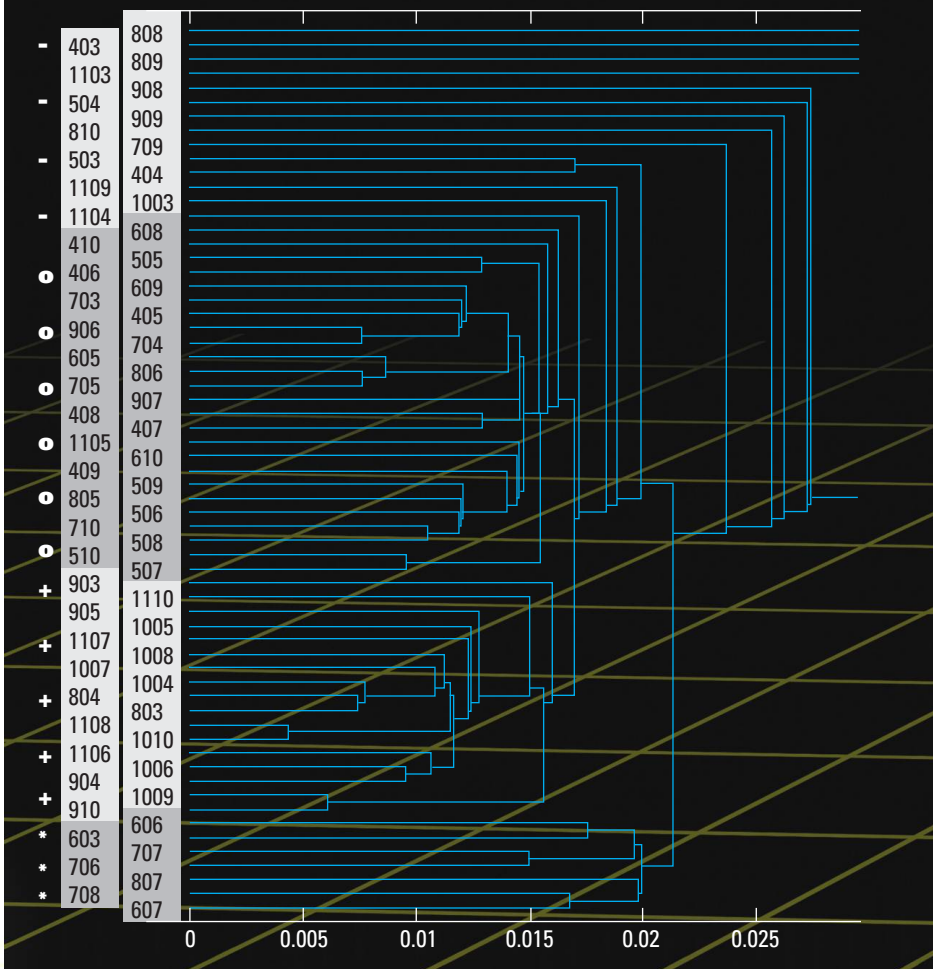


**FIGURE 5.** Hierarchical clustering of the MR data depicted in Figure 4.

The symbols on the left of the figure correspond with the symbols used in Figure 4. The horizontal axis represents the Euclidean distance in arbitrary units.

The MR spectra, as represented by the aforementioned input vectors, could roughly be divided into four different groups with the use of hierarchical clustering. The result of hierarchical clustering analysis is plotted as a dendrogram in Figure 5. Hierarchical clustering divides the data in large groups, which are then subdivided into smaller groups until all the "clusters" consist of only one sample. The division of the data is based on the distances between the input vectors. The Euclidean distance used in this particular patient study is a common distance measure.

PCA and LDA can also be used to cluster the MR spectra of different patients with brain tumors. These methods also use the six quantified resonances as input. With PCA, a set of linear combinations of the quantified peaks, called the principal components (PCs), is constructed in such a way that as much variation as possible is squeezed into the fewest possible new variables. The PCA score plot defined by the first two PCs yields a visualization of the spectra, which is based on the majority of the total information. With LDA, a set of linear combinations of the quantified peaks, called the discriminant functions, is constructed, which maximally separates the different groups of spectra labeled by the user. However, labeling of the spectra is problematic because accurate histological characterization of all spectroscopic voxels is often impossible.

Thus, overall, a reliable discrimination among brain tumors based on MRSI has yet to be accomplished, although progress has been made (*29*). Some clinical trial studies involving multiple sites have attempted to combine MRSI and MRI data to improve tumor discrimination.

## Prospects of combining MR images

On one hand, MRSI provides metabolic information at a low

spatial resolution; on the other hand, MRI provides morphological information on a high spatial resolution. The levels of metabolites differ in regions of the brain. For example, the MR spectra of normal (i) and malignant tumor (ii) tissue in Figure 4b clearly show differences. In addition, several studies have demonstrated that levels of NAA, Cr, and Cho differ between white matter and gray matter and may be affected by the contribution of cerebrospinal fluid (*30*–*32*). Therefore, to classify the spectra accurately, the MR spectra must be normalized to the tissue composition within the spectroscopic voxel.

Classifying the MR spectra on the basis of the estimated metabolite levels and the fraction of white matter, gray matter, cerebrospinal fluid, viable tumor, and necrosis within the spectroscopic voxel may be the best approach. Image and spectroscopic data are merged into one classifier or pattern recognizer. Several groups are developing an overall classifier of MR image and spectroscopic data (*33*). Such a classifier is also being developed at the University Medical Center Nijmegen, The Netherlands.

The measurement protocol involves the acquisition of the standard ρ-, $T_1$-, and $T_2$-weighted spin-echo images—a $T_1$-weighted spin-echo image after administering the contrast agent, a relative regional cerebral blood volume image, and a short echo-time spectroscopic image. The five MR images define a multispectral or multivariate image in which each pixel (image element) is characterized by its pixel intensities in the five MR images.

The multivariate image will be segmented into regions of white matter, gray matter, cerebrospinal fluid, viable tumor, and necrosis. Hopefully, patients will benefit from advanced evaluation and treatment by combining the segmented image with the spectroscopic image to improve the demarcation of the brain tumors from healthy tissue and the delineation of tissue heterogeneity within the tumor bed.

*Han Witjes and Arjan W. Simonetti are doctoral students at the University of Nijmegen, where Lutgarde Buydens chairs the analytical chemistry department. Witjes has research interests in chemometrics, NMR spectroscopy, and qualitative and quantitative analysis of spectra and images. Simonetti focuses research on spectral data analysis, image processing, and visualization of in vivo MRS and MRI data. Buydens examines almost all areas of chemometrics in her research. Address comments to Buydens at the Laboratory for Analytical Chemistry, University of Nijmegen, Toernooiveld 1, 6525 ED Nijmegen, The Netherlands or l.buydens@sci.kun.nl.*

## References

(1) Massart, D. L.; Vandeginste, B. G. M.; Buydens, L. M. C.; de Jong, S.; Lewi, P. J.; Smeyers-Verbeke, J. In *Handbook of Chemometrics and Qualimetrics: Vol. 20A, Part A;* Vandeginste, B. G. M., Rutan, S. C., Eds.; Elsevier Science Publishers: Amsterdam, 1998.

(2) Vandeginste, B. G. M.; Massart, D. L.; Buydens, L. M. C.; de Jong, S.; Lewi, P. J.; Smeyers-Verbeke, J. In *Handbook of Chemometrics and Qualimetrics: Vol. 20B, Part B;* Vandeginste, B. G. M., Rutan, S. C., Eds.; Elsevier Science Publishers: Amsterdam, 1998.

(3) Otto, M. *Chemometrics, Statistics and Computer Application in Analytical Chemistry;* Wiley-VCH: Weinheim, Germany 1999.

(4) Beebe, K. R.; Pell, R. J.; Seasholtz, M. B. *Chemometrics: A Practical Guide;* Wiley and Sons: New York, 1998.

(5) Gadian, D. G. *NMR and Its Applications to Living Systems;* Oxford University Press: Oxford, United Kingdom, 1995.

(6) Nelson, S. J.; Vigneron, D. B.; Dillon, W. P. *NMR Biomed.* **1999,** *12,* 123–138.

(7) Pratt, W. K. *Digital Image Processing;* Wiley & Sons: New York, 1978; pp 526–566.

(8) Evans, E. C.; Collins, D. L.; Neelin, P.; MacDonald, D.; Kamber, M.; Marret, T. S. In *Functional Neuroimaging: Technical Foundations;* Thatcher, R. W., Hallett, M., Zeffiro, T., John, E. R., Huerta, M., Eds.; Academic Press: Orlando, FL, 1994; pp 145–161.

(9) Alexander, M. E.; Somorjai, R. L.; *Magn. Reson. Imaging* **1996,** *14,* 453–468.

(10) Liang, Z.; Wang, D.; Ye, J.; Harrington, D. *IEEE Nuc. Sc. Symp.* **1995,** *3,* 1453–1456.

(11) Soltanian-Zadeh, H.; Windham, J. P.; Chen, F. *Automated contour extraction for medical image registration and segmentation.* Proceedings of SPIE Medical Imaging 1995: Image Processing Conference; Loew, M. H., Ed.; SPIE: San Diego, 1995.

(12) Soltanian-Zadeh, H.; Windham, J. P.; Peck, D. J.; Mikkelsen, T. *TPAMI* **1998,** *40,* 443–453.

(13) Perona, P.; Malik, J. *TPAMI.* **1990,** *12,* 629–639.

(14) Gerig, G.; Kubler, O.; Kikinis, R.; Jolesz. F. A. *IEEE Trans. Med. Imaging* **1992,** *11,* 221–232.

(15) Mohamed, F. B.; et al. *Proc. IEEE Eng. Med. Bio.* **1995,** *17,* 36–37.

(16) Geladi, P.; Grahn, H. *Multivariate Image Analysis;* Wiley & Sons: Chichester, United Kingdom, 1996.

(17) Geladi, P.; Isaksson, H.; Lindqvist, L.; Wold, S.; Esbensen, K. *Chemom. Intell. Lab. Syst.* **1989,** *5,* 209–220.

(18) Clarke, L. P.; et al. *Magn. Reson. Imaging* **1993,** *11,* 95–106.

(19) Vaidyanathan, M.; et al. *Magn. Reson. Imaging* **1995,** *13,* 719–728.

(20) Vaidyanathan, M.; et al. *Magn. Reson. Imaging* **1997,** *15,* 323–334.

(21) Klose, U. *Magn. Reson. Med.* **1990,** *14,* 26–30.

(22) de Beer, R.; van Ormondt, D. *NMR Basic Principles and Progress,* Vol. 26; Rudin, M., Ed.; Springer: Berlin, 1992; pp 201–248.

(23) Witjes, H.; et al. *J. Magn. Reson.* **2000,** *144,* 35–44.

(24) Marshall, I.; Higinbothan, J.; Bruce, S.; Freise, A. *Magn. Reson. Med .* **1997,** *37,* 651–657.

(25) Marquardt, D. W. *J. Soc. Ind. Appl. Math.* **1963,** *11,* 431–441.

(26) Bartha, R.; Drost, D. J.; Williamson P. C. *NMR Biomed.* **1999,** *12,* 205–216.

(27) Stoyanova, R.; Kuesel, A. C.; Brown, T. R. *J. Magn. Reson., Ser. A* **1995,** *115,* 265–269.

(28) Elliot, M. A.; Walter, G. A.; Swift, A.; Vandenborne, K.; Schotland, J. C.; Leigh, J. S. *Magn. Reson. Med.* **1999,** *41,* 450–455.

(29) Preul, M. C.; Caramanos, Z.; Leblanc, R.; Villemure, J. G.; Arnold, D. L. *NMR Biomed.* **1998,** *11,* 192–200.

(30) Wang, Y.; Li, S.-J. *Magn. Reson. Med.* **1998,** *39,* 28–33.

(31) Pouwels, P.; Frahm, J. *Magn. Reson. Med.* **1998,** *39,* 53–60.

(32) Noworolski, S. M.; et al. *Magn. Reson. Med.* **1999,** *41,* 21–29.

(33) Hetherington, H. P.; et al. *Magn. Reson. Med.* **1996,** *36,* 21–29.